

INVESTIGATION OF GROUND MOTIONS RECORDED DURING THE 2014 SOUTH NAPA EARTHQUAKE

Tadahiro Kishida¹, Silvia Mazzoni¹, Yousef Bozorgnia¹, Brian Chiou², Robert Darragh³,
Hamid R. Haddadi⁴, Robert Kayen⁵, Christopher Markham⁶, Sifat Muin¹, and Walt Silva³

¹Pacific Earthquake Engineering Research Center, University of California, Berkeley

²California Department of Transportation, Sacramento

³Pacific Engineering and Analysis, El Cerrito

⁴California Geological Survey, Sacramento

⁵US Geological Survey, Menlo Park and University of California, Berkeley

⁶Exponent, Oakland

Abstract

The 2014 South Napa mainshock caused significant damage in the Northern California Bay Area. Time series from a foreshock, mainshock, and three aftershocks were collected from various agencies. These were processed following the Pacific Earthquake Engineering Research Center (PEER) standard data-processing methods, and a ground-motion database was developed. Metadata such as fault style, source-to-site distance, average shear wave velocity in the top 30 m (V_{s30}), and basin depth were collected. Shear wave velocity profiles were also measured by the Spectral Analysis of Surface Wave Dispersion (SASW) technique at selected strong-motion stations. These datasets were combined in the ground motion database and compared to the Ground Motion Models (GMMs) from the NGA-West2 studies to evaluate the regional attenuation of these events. Time series at two geotechnical downhole array sites were also collected from 29 earthquakes to calculate apparent wave velocities from wave travel times and empirical transfer functions to understand wave amplification. Characteristics of pulse-like records from the South Napa and NGA-West2 databases were also analyzed to compare near-fault regions between these databases. The influence of pulse-like records was also investigated using inelastic response spectra to understand the damage potential on structures. These observed ground-motion characteristics are summarized in this study.

Introduction

The M6.0 South Napa earthquake occurred on August 24, 2014. The epicenter was located approximately 9 km south of the city of Napa in northern California. Residential structures and wineries surrounding this area were significantly damaged. After the earthquake, PEER summarized various preliminary observations, in which the following ground motion characteristics were described (Kishida et al. 2014a). In a comparison of the ground motion attenuation from the South Napa earthquake with the median NGA-West2 GMMs (e.g. Campbell and Bozorgnia 2014), the attenuation rate was higher from the South Napa event especially for relatively high-frequency 5% damped PSA. Baltay and Boatwright (2015) observed similar trends and noted that the northern California Bay Area has stronger attenuation compared to the average value of attenuation in the GMMs. To confirm these observations, the ground motion database was expanded by collecting the time series from one foreshock and three aftershocks of

the South Napa mainshock. The shear wave velocity profiles were also measured by the Spectral Analysis of Surface Wave Dispersion (SASW) technique at selected strong-motion stations. Combining these data, a ground motion database was developed to evaluate the regional attenuation in the northern California Bay Area.

The second characteristic observation was that two geotechnical downhole arrays operated by the California Strong Motion Instrumentation Program (CSMIP) in partnership with California Department of Transportation (Caltrans) (CE68206 and CE68259) located on the south side of the Carquinez Bridge (I-80) recorded PGAs of approximately 1g and 0.42g, respectively, during the 2014 South Napa mainshock. The hypocentral distance was approximately 20 km; hence the observed PGAs were unusually high compared to GMMs. These high PGAs were explained after the earthquake with potential causes such as local site effects, soil–structure interaction effects, or possible basin effects (Kishida et al. 2014a, Çelebi et al. 2015). Çelebi et al. (2015) analyzed the recorded time series and concluded that these large PGAs were caused by local site effects. To further understand wave propagation at the two downhole arrays, time series from 29 previous earthquakes also were collected from the Center for Engineering Strong Motion Data (CESMD 2014). Using this database, apparent wave velocities and empirical transfer functions (ETF) were calculated between sensors at different depths in the downhole arrays from wave travel times and ratios of Fourier amplitude spectrum (FAS), respectively.

The third characteristic was that pulse-like motions were observed in the velocity time series at several stations in near fault region. These large velocity pulses were observed during mainshock especially in the forward directivity direction (Kishida et al. 2014a). These pulses could possibly be related to the extensive damage observed at structures and wineries in the city of Napa. To understand these effects, we evaluated all the time series in the database for pulse characterization and compared these to the NGA-West2 database to define the region with potential damage from pulse-like velocity time histories. We also investigated the inelastic response spectra of the pulse-like waveforms to understand the pattern of observed damage during 2014 South Napa mainshock.

Ground Motion Database

Table 1 is the catalog of processed earthquakes in the South Napa sequence developed in this study. The moment magnitudes (**M**) were obtained from Northern California Earthquake Data Center (NCEDC). Hypocenter locations were similarly obtained from NCEDC using the double-difference method as described in Waldhauser and Ellsworth (2000). Time series were obtained from CESMD, Incorporated Research Institutions for Seismology (IRIS), NCEDC, and the California Department of Water Resource (CDWR). Approximately 1,350 records have been processed and filtered following the standard PEER data processing methods (Chiou et al. 2008, Ancheta et al. 2013) to provide uniformly processed time series, PSA at various dampings and Arias Intensity. Instrument corrections were also applied when the response of sensors was not directly proportional to acceleration. A time window for data processing was selected following the recommendations of previous studies (Goulet et al. 2014, Kishida et al. 2014b). An acausal Butterworth bandpass filter was applied after reviewing the FAS shape and the signal-to-noise ratio between the S-wave and the pre-event noise window (when available) on a component-by-component basis (e.g. Darragh et al. 2004, Chiou et al. 2008, Boore et al. 2012). 5%-damped

PSA were calculated at selected frequencies for all processed time series following Ancheta et al. (2013). The metadata from all the processing steps were also stored in the database such as record start time, location of station, time window locations, and applied high-pass and low-pass filter corner frequency. For approximately 500 stations in the database, estimates of V_{s30} were obtained from SASW performed for this study, the NGA-West2 study (Seyhan et al. 2014), or approaches that followed methodologies in the study by Seyhan et al. (2014) and Wills et al. (2015). The depths to bedrock were obtained from the USGS study (Aaggard et al. 2010). Directivity parameters were also obtained for the mainshock following the approach by Chiou and Youngs (2014) that used the finite fault model of Dreger et al. (2015).

Figures 1(a) – 1(c) show the attenuation of PGA, PSA(1.0s) and PSA(3.0s) with closest distance (R_{rup}) for the South Napa earthquake mainshock. The median of the four GMMs by Abrahamson et al. (2014), Boore et al. (2014), Campbell and Bozorgnia (2014), and Chiou and Young (2014) are also shown. At PGA, the median GMM prediction fits well to the observations at shorter distances ($R_{rup} < 20$ km), whereas it tends to over-predict as distance increase. At PSA of 1.0 and 3.0 s, the median prediction slightly underestimated the data at shorter distances, but fits better at greater distances. Baltay and Boatwright (2015) observed similar trends and explained that the over-prediction of high frequency at greater distance was due to the stronger regional attenuation in this area of northern California. Figures 1(d)-1(f) shows the residuals plotted on a regional map. Positive residuals become prominent in the region north of the mainshock epicenter as period increases. Figures 1(g)-1(i) show the residuals against delta DPP which was the directivity indicator used by Chiou and Youngs (2014). Clear directivity effects were observed in these figures for PSA(3.0s). These effects become unclear as period decreases. Baltay and Boatwright (2015) similarly observed positive correlations with residuals against DPP. Figures 1(j) – 1(l) show the attenuation of PGA with closest distances (R_{rup}) for the three aftershocks. Stronger attenuation with distance were also observed for all three events compared to the median GMM with R_{rup} .

Table 1. Catalog for the South Napa earthquake sequence in the PEER Database

Earthquake Name	Origin Time (Year-Mo-DyTHr:Mn:Sc)	Latitude (°N)	Longitude (°E)	Depth (km)	M
Foreshock	2014-08-05T12:40:01	38.2557	-122.323	8.20	3.03
Mainshock	2014-08-24T10:20:44	38.21517	-122.312	11.12	6.02
Aftershock1	2014-08-24T12:47:12	38.23833	-122.343	8.439	3.60
Aftershock2	2014-08-26T12:33:16	38.1785	-122.301	12.577	3.90
Aftershock3	2014-08-31T08:56:20	38.23583	-122.329	9.55	3.24

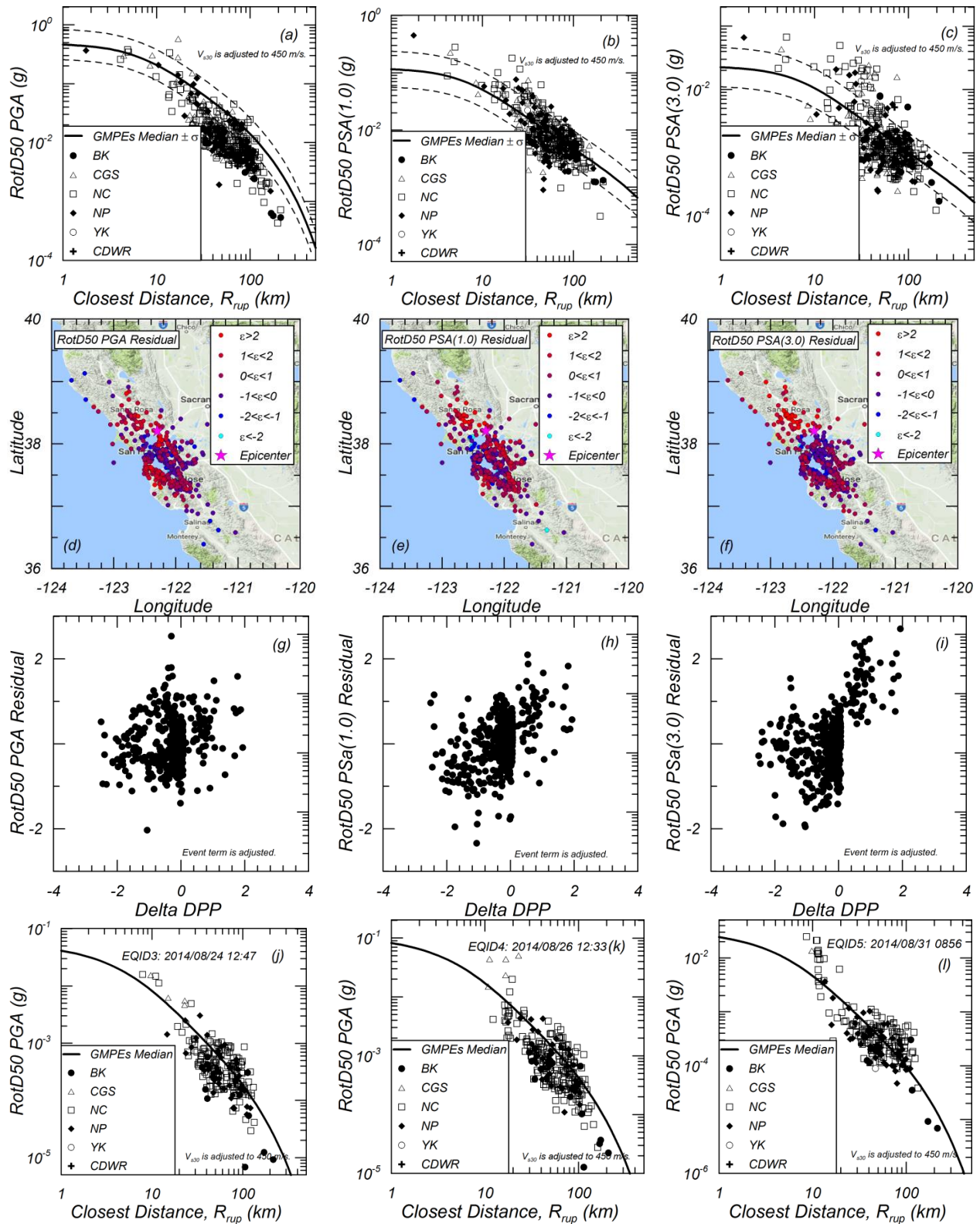


Figure 1. Variations in (a) PGA, (b) PSA(1.0s), (c) PSA(3.0s) against R_{rup} , variations in residuals of (d)PGA, (e) PSA(1.0s) and (f)PSA(3.0s) on a map, variations in residuals of (g) PGA, (h) PSA(1.0) and (i) PSA(3.0) against Delta DPP for 2014 South Napa mainshock, variations in PGA for three aftershocks (j)EQID3, (k) EQID4, and (l) EQID5 against R_{rup} .

Site Characterization of Strong-Motion Stations by SASW

SASW were performed at 15 strong-motion stations. Table 2 lists these stations, which were selected based on the several factors such as number of recordings in the database, the significance of the strong shaking during the mainshock, and velocity information available in NGA-West2 site database (Seyhan et al. 2013). Figure 2 show pictures of a typical SASW layout. Figure 3 shows an example of the surface wave dispersion curves produced by SASW at the geotechnical downhole array at the south end of the Carquinez Bridge. Surface waves were generated by a truck and recorded by a linear array of seismometers. Figure 4 shows the comparison of the V_s profile from SASW to the suspension logging results from CSMIP (CESMD 2014). These two V_s profiles agree well at depth, while the SASW method provides V_s measurements to the surface.

Table 2. Station list of V_s measurements by SASW

Station Name	Network	Station ID	Latitude (°N)	Longitude (°E)	# of records
Napa - Napa College	CGS	68150	38.270	-122.277	4
Green Valley Road	NC	NGVB	38.280	-122.216	4
Huichica Creek	NC	NHC	38.217	-122.358	5
Lovall Valley Loop Rd	NC	N019B	38.301	-122.402	4
Oakmont	NP	1835	38.442	-122.607	4
Martinez	NP	1847	38.0130	-122.134	4
Glen Ellen	NP	1848	38.367	-122.524	4
McCall Drive, Benicia, CA	NC	C032	38.083	-122.158	5
Main St, Napa, CA	NP	N016	38.299	-122.285	5
Vallejo_FD	NP	1759	38.108	-122.256	2
Napa; Fire Station No. 3	NP	1765	38.330	-122.318	2
NMI	NC	NMI	38.076	-122.259	2
Sonoma	NP	1829	38.290	-122.461	3
Old Carquinez Bridge north free-field	CGS	68184	38.0675	-122.226	1
Carquinez Bridge Geotechnical Array	CGS	68206	38.056	-122.226	3



Figure 2. Example pictures of SASW testing equipment

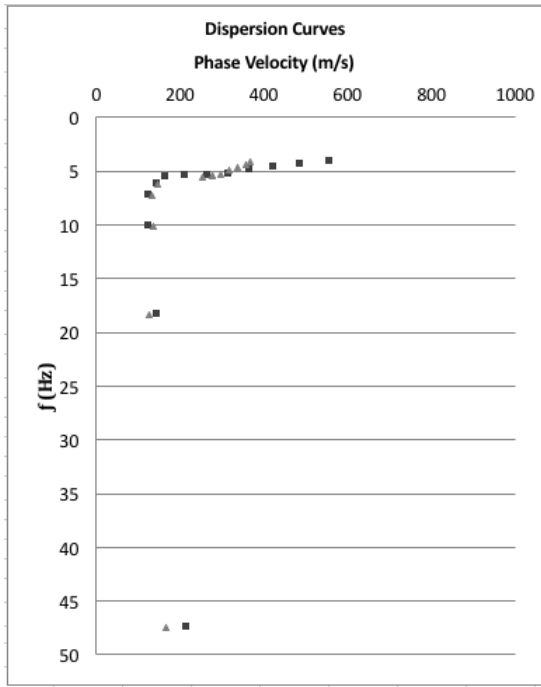


Figure 3. Surface wave dispersion curves at Carquinez Bridge Geotechnical Array (68206)

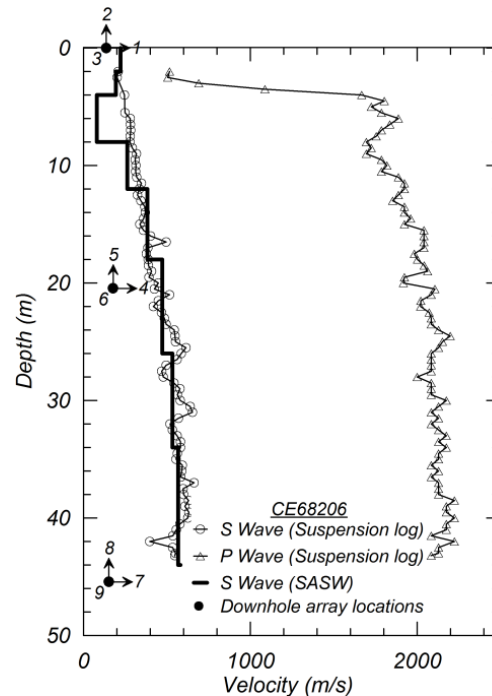


Figure 4. Comparison of the SASW Vs profile with suspension logging results

Carquinez Bridge Geotechnical Array Recordings

The Carquinez Bridge geotechnical array (CE68206) recorded peak ground acceleration of approximately 1.0g at ground surface during 2014 South Napa earthquake. To understand this observation downhole records were collected and processed from 29 previous earthquakes at this array and the nearby CE68259 array. The apparent wave velocities between sensors at depth and empirical wave amplification were estimated. Table 3 lists these earthquakes for which magnitude ranged from 2.2 to 6.0.

Apparent Wave Velocities

Apparent V_s and V_p were calculated between downhole recordings by computing wave travel times. Two analyses were conducted to calculate these velocities. The first was cross-correlation method (CCM) (e.g. Elgamal et al. 1995), and the second was the normalized input-output method (NIOM) (Haddadi and Kawakami, 1998). Incident P- and S-wave-travel times were only considered in the analyses. Figure 5a shows the comparison of apparent wave velocities with field measurements for both of the geotechnical arrays. It shows reasonable agreement between apparent wave velocities and field measurements, where 91% of velocity measurements from CCM and NIOM were within $\pm 30\%$ of the measured velocity. Figure 5b shows the same dataset, however, the x-axis is the difference in apparent velocities between CCM and NIOM methods. The data with large differences between apparent and measured wave velocities also have large differences between the values from CCM and NIOM. Therefore, these data were removed from further analyses when the differences between CCM and NIOM were

greater than 30%. This screening process reduced the percentage of erroneous data (i.e. the difference greater than 30% from the measured velocity) from 9% to 2%.

Table 3. Earthquakes recorded at geotechnical downhole arrays (CE68206 and CE68259)

Earthquake Name	Origin Time (Year-Mo-DyTHr:Mn:Sc)	Earthquake Location	Latitude (°N)	Longitude (°E)	Depth (km)	M
1	2006-08-03T03:08:12.86	Glen Ellen	38.3635	-122.589	8.55	4.5
2	2006-12-21T03:12:28.76	Berkeley	37.85717	-122.245	8.643	3.6
3	2007-03-02T04:40:00.75	Lafayette	37.8965	-122.111	15.981	4.23
4	2007-07-20T11:42:22.36	Oakland	37.804	-122.193	5.262	4.2
5	2007-10-31T03:04:54.81	Alum Rock	37.4335	-121.774	9.741	5.45
6	2008-06-04T02:29:04.15	Green Valley	38.24183	-122.184	10.065	3.96
7	2008-09-06T04:00:15.25	Alamo	37.862	-122.008	16.328	4.1
8	2011-01-08T00:10:16.74	Seven Trees	37.28717	-121.658	9.593	4.1
9	2011-08-24T16:57:44.12	San Leandro	37.74517	-122.151	8.632	3.38
10	2011-10-20T21:41:04.26	Berkeley	37.857	-122.253	7.989	3.95
11	2011-10-21T03:16:05.26	Berkeley	37.86083	-122.257	7.939	3.84
12	2011-10-27T12:36:44.46	Berkeley	37.86666	-122.261	7.99	3.62
13	2012-02-16T02:09:14.05	Crockett	38.07667	-122.233	8.827	3.55
14	2012-02-16T17:13:20.58	Crockett	38.07817	-122.234	8.247	3.54
15	2012-03-16T02:56:49.65	Crockett	38.07367	-122.23	7.464	2.48*
16	2014-01-14T04:18:17.60	Vallejo	38.0985	-122.238	8.157	2.76*
17	2014-04-28T21:53:24.41	Vallejo	38.093	-122.253	8.024	2.23*
18	2014-08-24T10:20:44.07	American Canyon	38.21517	-122.312	11.12	6.02
19	2014-08-24T12:47:12.55	Napa	38.23833	-122.343	8.439	3.6
20	2014-08-26T00:02:34.67	Napa	38.24033	-122.341	6.927	2.79*
21	2014-08-26T12:33:16.84	American Canyon	38.1785	-122.301	12.577	3.9
22	2014-08-26T12:35:52.99	American Canyon	38.17567	-122.307	11.473	2.7*
23	2014-08-26T13:12:19.96	American Canyon	38.17933	-122.297	10.006	2.71*
24	2014-08-31T08:56:20.83	Napa	38.23583	-122.329	9.55	3.24
25	2014-09-01T01:41:14.29	American Canyon	38.17717	-122.31	9.141	2.47*
26	2014-09-04T10:56:23.17	American Canyon	38.18033	-122.303	10.937	2.93*
27	2014-09-29T07:17:01.22	American Canyon	38.177	-122.303	11.711	2.5*
28	2015-04-01T14:07:47.16	San Pablo	37.97017	-122.352	4.85	2.67*
29	2015-04-02T07:06:03.87	San Ramon	37.792	-121.987	9.89	3.61

*Magnitude is obtained from Md.

Apparent V_s were calculated by varying the azimuthal angles (rotated by 1°) from the two horizontal time series. Figures 6(a) and (b) show the variation in apparent V_s near the ground

surface with azimuthal angle for CE68206 and CE68259, respectively. The results show the clear negative correlation of apparent velocities with the PGA along the rotated azimuthal angle in the mainshock. Figure 7(a) and (b) show the variation of apparent wave velocity with PGA for the two geotechnical arrays from all the earthquakes. It shows that the wave velocity decreases near the ground surface as PGA increases, which may indicate nonlinear soil behavior due to strong shaking. ETFs are also calculated at CE68206 and CE68259 and compared with the theoretical transfer functions (TTF) in Figure 8(a) and (b), respectively. The figure shows good agreement between these two transfer functions, especially for the resonance modes, although the amplification factors are different between these due to differences in damping. During the South Napa mainshock, there is a clear broadening of resonance periods near 6-10 Hz at CE68206.

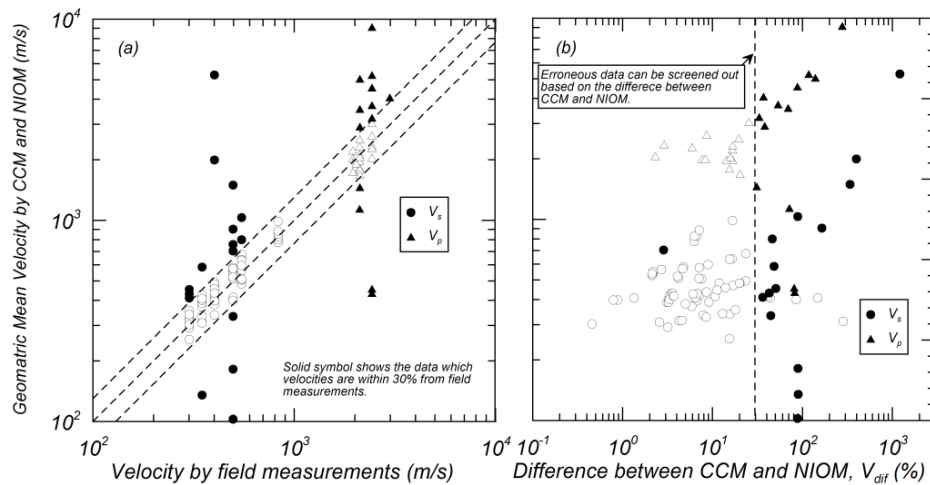


Figure 5. Comparison of apparent wave velocities (a) with field measurements (b) between CCM and NIOM.

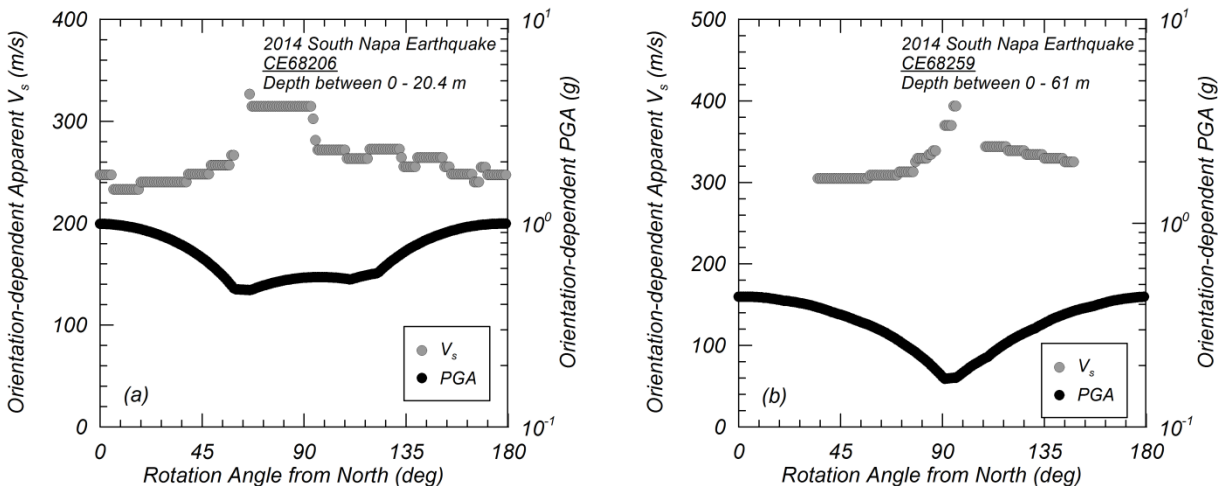


Figure 6. Variation in apparent V_s depending on rotation angle with PGA at (a) CE68206 and (b) CE68259 during the 2014 South Napa earthquake.

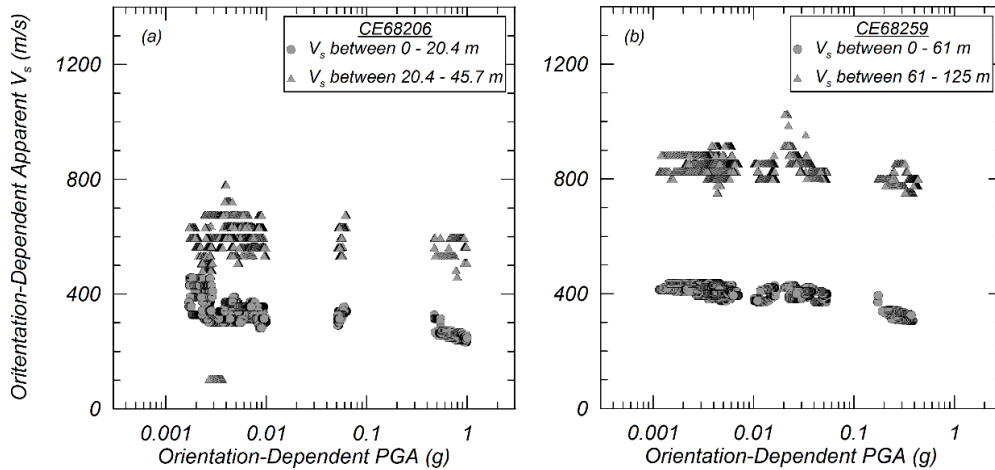


Figure 7. Variation in apparent V_s against PGA at (a) CE68206 and (b) CE68259.

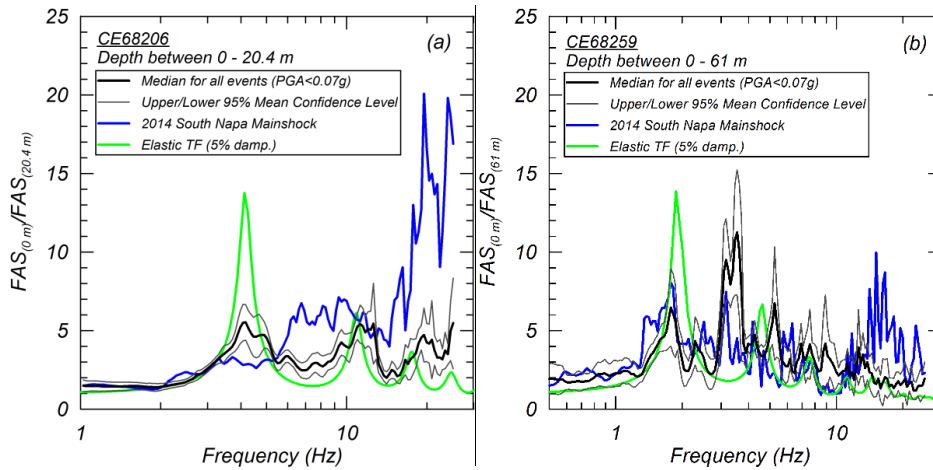


Figure 8. Empirical transfer functions at (a) CE68206 and (b) CE68259.

Identification of Velocity Pulses for Near-Fault Records

Pulses in the velocity time history were observed at near fault stations during the mainshock of the 2014 South Napa earthquake (Kishida et al. 2014a). After the development of the ground motion database, the entire database was analyzed to identify pulse-like records. The methodologies developed by Hayden et al. (2014) and Shahi and Baker (2014) were implemented and compared. Table 4 shows a summary of the recordings identified as pulse-like records in South Napa database; all pulse-like recordings were from the mainshock. A pulse was identified at 7 stations by at least one of the two methods. Differences exist in the calculated pulse period as well as the pulse azimuth (i.e., azimuth of max pulse and azimuth of max peak-to-peak for the Shahi and Baker 2014 and Hayden et al. 2014 methods, respectively) presented in Table 4.

Figure 9 shows example velocity time series, which were identified as pulse-like recordings by both methods. The time series were rotated to the azimuthal angle in which the pulse characteristics were identified. This figure shows maximum velocities of approximately 80 cm/s and clear velocity pulses in both recordings. Figure 10 shows the locations of the stations

where the pulse-like records were identified by either method. Most of the stations were located in the forward directivity region of the fault rupture (e.g. Dreger et al. 2015), whereas the Vallejo – Broadway & Sereno recording site was located in the backward directivity region. The Vallejo – Broadway & Sereno station has a calculated pulse period less than 1.0 s for both methods whereas the other stations in the forward directivity region have pulse periods greater than 1.0 s. The distribution of stations in Figure 10 largely overlaps the station distributions with large positive residuals of PSA (3.0s) in Figure 1(f).

Pulse-like recordings were strongly related to directivity effects in these plots. Similar identifications of pulse-like recordings were performed for the NGA-West2 database (Ancheta et al. 2013). Figure 11 shows scatter plot (R_{rup} versus M) of identified pulse-like recordings in the South Napa and NGA-West2 databases. The pulse-like recordings were observed generally within R_{rup} less than 10 km for M 5. There was a trend for R_{rup} to increase as M increases which could be used to define the near-fault region for design practice.

Table 4. Pulse Identification for recordings from the 2014 South Napa Mainshock

Station Name	RSN	Hayden et al. (2014)			Shahi and Baker (2014)		
		Pulse Identified	Azimuth of Max PPV* (°)	Pulse Period (s)	Pulse Identified	Azimuth of Max Pulse (°)	Pulse Period (s)
Napa College	51	No	160	1.6	Yes	154	2.0
Huichica Creek	89	Yes	171	5.5	Yes	166	2.8
Lovall Valley Loop Rd.	212	Yes	61	3.8	Yes	69	3.6
Fire Station No. 3	217	Yes	62	3.8	Yes	29	4.4
Main St. Napa	219	Yes	56	3.4	No	60	3.9
Atlas Peak	702	Yes	103	2.0	No	177	2.4
Vallejo - Broadway & Sereno	1318	Yes	45	0.6	No	50	0.6

* PPV = Peak-to-Peak Velocity (Hayden et al. 2014)

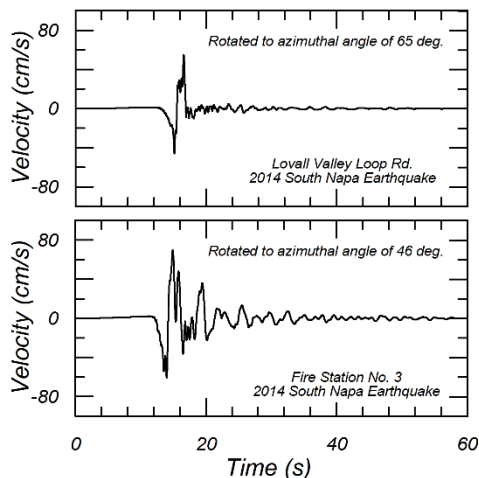


Figure 9. Example of pulse-like time series recorded in the South Napa mainshock.

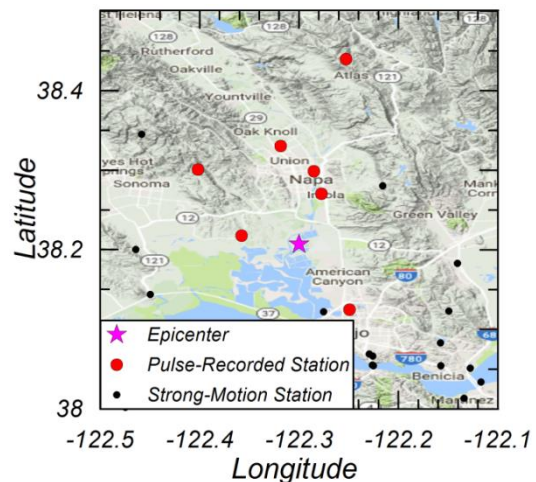


Figure 10. Locations of stations with pulse-like records identified in the 2014 South Napa mainshock.

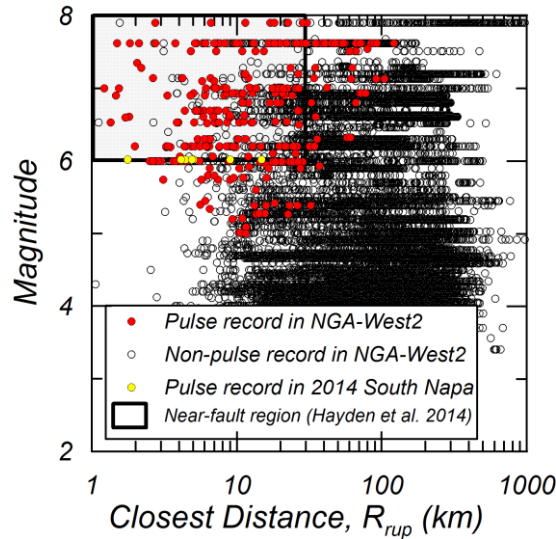


Figure 11. Distribution of pulse-like recordings in the NGA-West2 and South Napa database

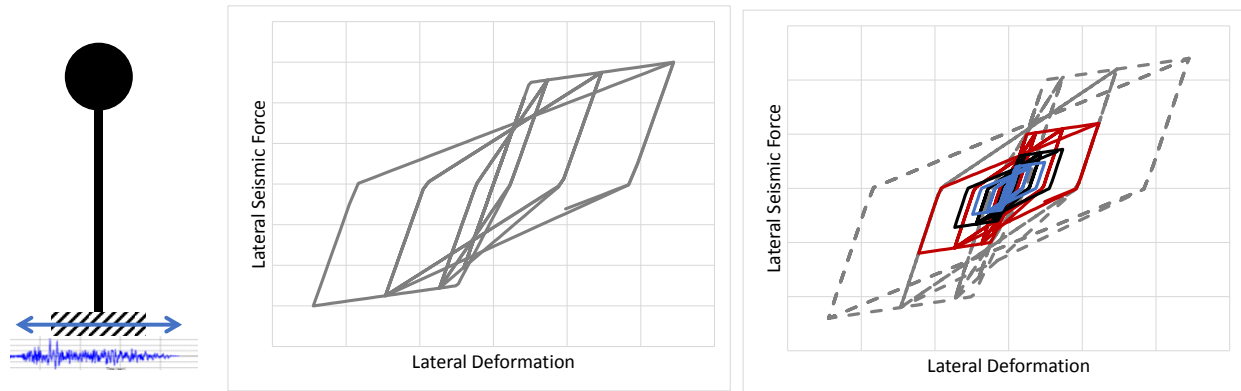


Figure 12. Inelastic-Response Model

Pulse-Motion Characteristics by Inelastic Spectra

Inelastic response spectra were computed for the pulse motions to determine whether the presence of the pulse affected the response of an inelastic system and whether the period shift associated with inelasticity affected the response. The generalized inelastic SDOF model that was used in the analysis is shown in Figure 12, with the analyses performed using OpenSees (McKenna, 1997). This generalized model is consistent with what is assumed in ASCE 7-16. This model was chosen because it represents the critical characteristics of inelastic response – nonlinearity, hysteresis, strength and stiffness degradation due to cycling and ductility. The inelastic spectra were computed for a range of periods and strengths, as shown in Figure 12.

The strength parameter that was used in the analysis is the Estimated-Strength Reduction Factor, R_d , defined as the ratio between the elastic lateral-force demand for design ($2/3 MCE_R$) and the yield strength of the structure, V_y . This value is equivalent to a combination of the strength-reduction factor R and the strength-amplification factor Ω used in design. (R_d Range:

0.5-10) ($R_d > 1$: structure will yield below $2/3 MCE_R$, $R_d < 1$: structure will remain elastic below $2/3 MCE_R$). It is important to note that with this definition of R_d , the estimated yield strength of the structure is defined as a function of the site-specific design spectrum. The MCE_R spectrum was computed for each recording station. A graphical representation of the effect of R_d on the design spectra is shown in Figure 13. Because inelastic response of very-stiff structures may yield questionable results, the inelastic spectra were computed for a period range between 0.1 and 10 seconds.

The spectral displacement computed in the inelastic response spectra was normalized to a ductility value to make a graphic comparison over all periods. The inelastic-spectra for two recording stations, “Napa College, RSN 51, JB Dist=3.1 km” and “Lovall Valley Loop Rd, RSN 212, JB Dist=5.0 km”, are shown in Figure 14 and 15, respectively, because they display interesting response characteristics. The Napa College record has a pulse at a period between 1 and 2 seconds. This pulse is identified by both identification methods and is evident in the elastic response spectrum, in the Fault-Parallel direction, as shown in Figure 14, top-left figure. The remaining graphs in the figure plot the displacement ductility versus initial elastic period for the Fault-Normal and Fault-Parallel directions, as well as for the azimuth direction for both the Hayden and Shahi pulse characterizations. Each of these inelastic spectra plots the response for different cases of Estimated-Strength Reduction Factor. Figure 14 show that the pulse shape is identified for the cases where the response is near yield (ductility=1, $R_d < 2$). However, for the cases of larger strength reduction, the pulse shape is no longer observed and high ductility demands are evident in all periods below 3 seconds.

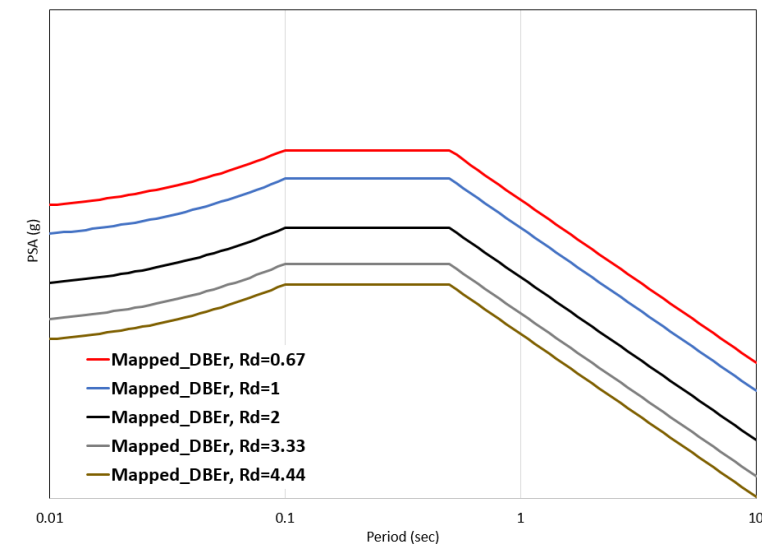


Figure 13. Inelastic Design Spectra

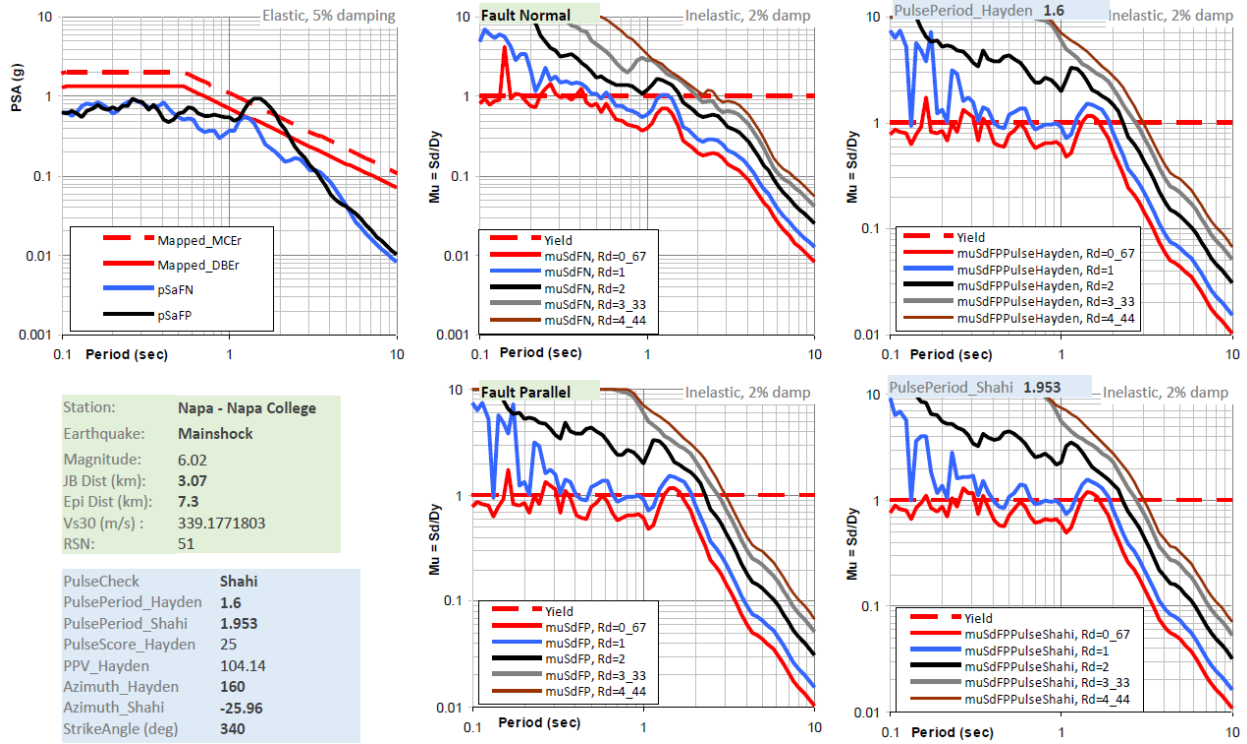


Figure 14. Inelastic Spectra for Napa College, RSN 51, JB Dist=3.1 km

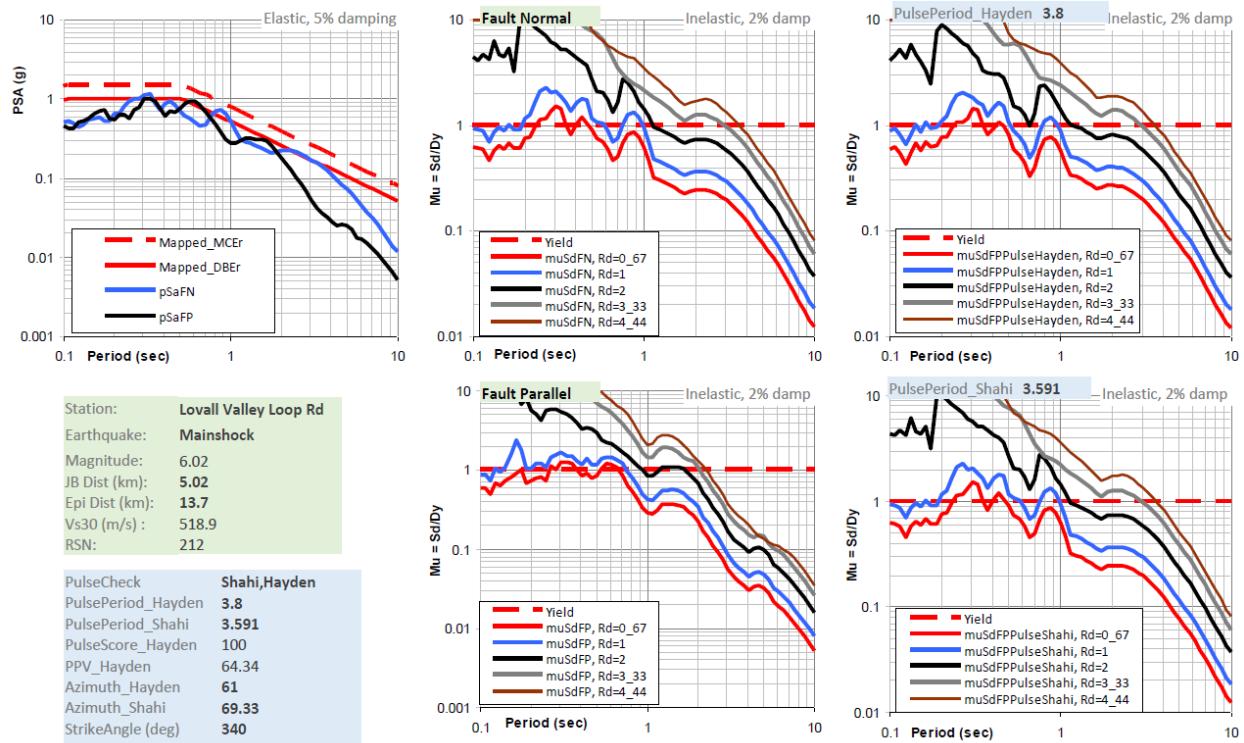


Figure 15. Inelastic Spectra for Lovall Valley Loop Rd, RSN 212, JB Dist=5.0 km

The inelastic spectra for the Lovall Valley Loop Rd record show that the pulse at between 3 and 4 seconds, identified by both methods and observed in the Fault-Normal response, does affect the inelastic response in that period range. The low levels of ductility demand for the cases of the structures with the lowest strength, however, indicate that the pulse does not cause collapse of the structure, unless its ductility capacity is very low. An evaluation of all inelastic response spectra, however, do indicate that the structures at highest risk at the shorter-period structures. This assessment needs to be verified through a rigorous comparison with the response of records without pulse characteristics.

Conclusions

Ground motion characteristics of the 2014 M6.0 South Napa earthquake have been investigated. The ground motion database was developed by collecting the time series from one foreshock, mainshock and three aftershocks from various agencies. Shear wave velocity profiles were also measured by the Spectral Analysis of Surface Wave Dispersion (SASW) technique at 15 selected strong-motion stations. Combining these data, a ground motion database was developed, and compared to GMMs in NGA-West2 studies. The results show the stronger attenuation of PGA for these events compared to the median of NGA-West2 models, indicating regional attenuation in this region of northern California Bay Area is greater than predicted by the average GMM. This observation was similar to those by Baltay and Boatwright (2015). The study also reviewed time histories from the two geotechnical downhole arrays operated at the south side of the Carquinez Bridge (I-80), which recorded PGAs of approximately 1g and 0.42g, respectively, during the 2014 South Napa mainshock. The apparent wave velocities computed from the downhole arrays show the clear reduction in V_s during mainshock, indicating that reduction of soil stiffness occurred due to strong shaking. The ETFs were also computed from downhole records and compared to the TTF from V_s profiles. The comparison shows good agreement of resonance periods especially at CE68206, where the maximum PGA of 1g was recorded. The ETF also shows the clear broadening of resonance periods at CE68206 during mainshock, which is consistent to the reduction of V_s in apparent wave velocities. Therefore, evaluations based on one-dimensional wave propagation reasonably explain the downhole array observations in mainshock, which is consistent with the results of Çelebi et al. (2015).

The pulse-like velocity time series were investigated by using Hayden et al. (2014) and Shahi and Baker (2014) approaches and utilizing the South Napa and NGA-West2 databases developed in this study. In the South Napa earthquakes, 7 records from mainshock are identified as pulse-like, where most of these stations were located in the forward directivity region. The pulse periods estimated by these two methods were mainly between 2.0 – 4.4 s. The distributions of these stations were consistent with the regions where the positive residuals were observed for PSA(3.0s) compared with GMMs from NGA-West2 studies. The comparison of near-fault regions by pulse-like records between South Napa earthquake and NGA-West2 database also showed that these are reasonably consistent, and increase as magnitude increases. Inelastic response spectra for the recorded ground motions can be used to gain further insight into the expected response of structures with different stiffness (period) and strength characteristics.

Acknowledgements

The project acknowledges Tony Shakal and Moh Huang (CSMIP) for providing the suspension profiles, boring logs and numerous discussions. The assistance by Tom Shantz, Caltrans, who assisted with access at the Carquinez Bridge SASW sites is greatly appreciated. The authors also acknowledge Prof. Stewart and Dr. Gutierrez for providing V_{s30} estimates, and Dr. Aagaard for basin depths at strong-motion stations. The project is funded by CSMIP and the California Department of Transportation and those funds are gratefully acknowledged. The views and conclusions contained in this document are those of the authors and should not be interpreted as necessarily representing the above organizations

Reference

- Aagaard B.T., Graves R.W., Rodgers A., Brocher T.M., Simpson R.W., Dreger D., Petersson N.A., Larsen S.C., Ma S., Jachens R.C. (2010). Ground-motion modeling of Hayward fault scenario earthquakes, Part II: Simulation of long-period and broadband ground motions, *Bull. Seismol. Soc. Am.*, 100(6): 2945–2977.
- Abrahamson, N. A., Silva, W. J., and Kamai, R., 2014. Summary of the Abrahamson, Silva, and Kamai NGA-West2 ground-motion relations for active crustal regions, *Earthquake Spectra* 30, 1025–1055.
- Ancheta, T. D., Darragh, R. B., Stewart, J. P., Seyhan, E., Silva, W. J., Chiou, B. S.J., Wooddell, K. E., Graves, R. W., Kottke, A. R., Boore, D. M., Kishida, T. Donahue, J. L. (2013), "PEER NGA-West2 Database", Pacific Earthquake Engineering Research Center, PEER Report 2013/03.
- Baltay, A. S. and Boatwright, J. (2015). Ground-Motion Observations of the 2014 South Napa Earthquake, *Seismological Research Letters* Volume 86, Number 2A, doi: 10.1785/0220140232.
- Boore, D. M., A. Azari Sisi, and S. Akkar (2012). Using pad-stripped acausally filtered strong-motion data, *Bull. Seismol. Soc. Am.* 102 751-760.
- Boore, D.M., J.P. Stewart, E. Seyhan, and G.M. Atkinson (2014). NGA-West 2 equations for predicting PGA, PGV, and 5%-damped PSA for shallow crustal earthquakes, *Earthquake Spectra* 30, 1057-1085.
- Bozorgnia, Y., Abrahamson, N. A., Atik, L. A., Ancheta, T. D., Atkinson, G. M., Baker, J. W., Baltay, A., Boore, D. M., Campbell, K. W., Chiou, B. S.-J., Darragh, R., Day, D., Donahue, J., Graves, R. W., Gregor, N., Hanks, T., Idriss, I. M., Kamai, R., Kishida, T., Kottke, A., Mahin, S. A., Rezaeian, S., Rowshandel, B., Seyhan, E., Shahi, S., Shantz, T., Silva, W., Spudich, P., Stewart, J. P., Watson-Lamprey, J., Wooddell, K., and Youngs, T. (2014). "NGA-West2 Research Project". *Earthquake Spectra*, EERI, August 2014, Vol. 30, No. 3, pp. 973-987.
- Campbell, K. W., and Bozorgnia, Y., (2014). NGA-West2 ground motion model for the average horizontal components of PGA, PGV, and 5%-damped linear Response Spectra, *Earthquake Spectra* 30, 1087–1115.

- Çelebi, M., Ghahari, S. F. and Taciroglu, E. (2015), Unusual Downhole and Surface Free-Field Records Near the Carquinez Strait Bridges during the 24 August 2014 Mw 6.0 South Napa, California, Earthquake, *Seismological Research Letters* Volume 86, Number 4. doi: 10.1785/0220150041.
- CESMD (Center for Engineering Strong Motion Data) (2014), <http://www.strongmotioncenter.org/> (last accessed September 2016).
- Chiou, B. S.-J., and Youngs, R. R., (2014). Update of the Chiou and Youngs NGA ground motion model for average horizontal component of peak ground motion and response spectra, *Earthquake Spectra* 30, 1117–1153.
- Chiou, B., Darragh, R., Gregor, N., and Silva, W. (2008), NGA project strong-motion database, *Earthquake Spectra*, Vol. 24, No. 1, pp. 23–44.
- Darragh B, Silva W, Gregor N (2004) Strong motion record processing procedures for the PEER center. In: *Proceedings of COSMOS workshop on strong-motion record processing*. Richmond, California, pp 1–12.
- Dreger, D. S., Huang, M.-H., Rodgers, A., Taira, T. and Wooddell, K. (2015), Kinematic Finite-Source Model for the 24 August 2014 South Napa, California, Earthquake from Joint Inversion of Seismic, GPS, and InSAR Data, *Seismological Research Letters* Volume 86, Number 2A, pp327-334, doi: 10.1785/0220140244.
- Elgamal, A. W., Zeghal, M., Tang, H. T. and Stepp, J. C., “Lotung Downhole Array. I: Evaluation of Site Dynamic Properties”, *J. Geotech. Engrg.*, 1995, 121(4): 350-362.
- Goulet, C. A., Kishida, T., Cramer, C. H., Darragh, R. B., Silva, W. J., Hashash, Y. M. A., Harmon, J., Stewart, J. P., Wooddell, K. E., Youngs R. R. (2014), "PEER NGA-East Database", Pacific Earthquake Engineering Research Center, PEER Report 2014/09.
- Haddadi, H. R. and Kawakami, H. (1998), Modeling Wave Propagation by using Normalized Input-Output Minimization (NIOM) Method for Multiple Linear Systems, *Doboku Gakkai Ronbunshu*, Vol. 1998 (1998) No. 584 P 29-39
- Hayden, C. P., Bray, J. D. and Abrahamson, N. A. (2014), Selection of Near-Fault Pulse Motions, *J. Geotech. Geoenviron. Eng.*, 2014, 140(7): 04014030.
- Kishida, T., Kayen, R.E., Ktenidou, O.-J., Silva, W.J., Darragh, R.B. and Watson-Lamprey, J. (2014b), PEER Arizona Strong-Motion Database and GMPEs Evaluation, Pacific Earthquake Engineering Research Center, University of California, Berkeley, CA, PEER Report 2014/09.
- Kishida, T., Wang, S., Mazzoni, S., Markham, C., Lu, Y., Bozorgnia, Y., Mahin, S, Bray, J., Panagiotou, M., Stewart, J., Darragh, R., Abrahamson, N., Hollenback, J., Gutierrez, C., Chiou, B., Muin, S., Dreger, D. (2014a), "PEER Preliminary Notes and Observations on the August 24, 2014, South Napa Earthquake, 1. Strong motion records", Pacific Earthquake Engineering Research Center, PEER Report 2014/09.
- Seyhan E, Stewart JP, Ancheta TD, Darragh RB, Graves RW (2014): NGA-West2 Site Database. *Earthquake Spectra*, 31(3), 1007-1024.

- Shahi, S. K. and Baker, J. W. (2014), An Efficient Algorithm to Identify Strong-Velocity Pulses in Multicomponent Ground Motions, *Bulletin of the Seismological Society of America*, Vol. 104, No. 5, pp. 2456–2466.
- Waldhauser, F. and Ellsworth, W. L. (2000), A Double-Difference Earthquake Location Algorithm: Method and Application to the Northern Hayward Fault, California, *Bulletin of the Seismological Society of America*, 90, 6, pp. 1353–1368, December 2000.
- Wills, C. J., Gutierrez, C. I., Perez, F. G. and Branum, D. M. (2015), “A Next Generation VS30 Map for California Based on Geology and Topography”, *Bulletin of the Seismological Society of America*, Vol. 105, No. 6, pp. –, December 2015, doi: 10.1785/0120150105.

